Amino Acids (2010) 39:565–578
DOI 10.1007/s00726-010-0475-9

ORIGINAL ARTICLE

Biochemical characteristics and inhibitor selectivity of mouse indoleamine 2,3-dioxygenase-2

Christopher Jonathan Daraius Austin · B. M. Mailu · G. J. Maghzal · A. Sanchez-Perez · S. Rahlfs · K. Zocher · H. J. Yuasa · J. W. Arthur · K. Becker · R. Stocker · N. H. Hunt · H. J. Ball

Received: 24 August 2009 / Accepted: 6 January 2010 / Published online: 7 February 2010

Abstract The first step in the kynurenine pathway of tryptophan catabolism is the cleavage of the 2,3-double bond of the indole ring of tryptophan. In mammals, this reaction is performed independently by indoleamine 2,3-dioxygenase-1 (IDO1), tryptophan 2,3-dioxygenase (TDO) and the recently discovered indoleamine 2,3-dioxygenase-2 (IDO2). Here we describe characteristics of a purified recombinant mouse IDO2 enzyme, including its pH stability, thermal stability and structural features. An improved assay system for future studies of recombinant/isolated IDO2 has been developed using cytochrome b_5 as an electron donor. This, the first description of the interaction between IDO2 and cytochrome b_5, provides further evidence of the presence of a physiological electron carrier necessary for activity of enzymes in the "IDO family". Using this assay, the kinetic activity and substrate range of IDO2 were shown to be different to those of IDO1. 1-Methyl-D-tryptophan, a current lead IDO inhibitor used in clinical trials, was a poor inhibitor of both IDO1 and IDO2 activity. This suggests that its immunosuppressive effect may be independent of pharmacological inhibition of IDO enzymes, in the mouse at least. The different biochemical characteristics of the mouse IDO proteins suggest that they have evolved to have distinct biological roles.

Keywords Cytochrome b_5 · Oxidation/reduction · Electron donation · IDO2

C. J. D. Austin and B. M. Mailu contributed equally to the work in this paper.

Electronic supplementary material The online version of this article (doi:10.1007/s00726-010-0475-9) contains supplementary material, which is available to authorized users.

C. J. D. Austin · A. Sanchez-Perez · N. H. Hunt · H. J. Ball (✉)
Molecular Immunopathology Unit,
Discipline of Pathology and Bosch Institute,
University of Sydney, Camperdown,
NSW 2006, Australia
e-mail: helenb@med.usyd.edu.au

B. M. Mailu · S. Rahlfs · K. Zocher · K. Becker
Interdisciplinary Research Center,
Giessen University, Giessen, Germany

G. J. Maghzal · R. Stocker
Centre for Vascular Research, School of Medical Sciences (Pathology) and Bosch Institute, Sydney Medical School, University of Sydney, Sydney, NSW, Australia

H. J. Yuasa
Laboratory of Biochemistry, Department of Applied Science, Faculty of Science, National University Corporation Kochi University, Kochi 780-8520, Japan

J. W. Arthur
Discipline of Medicine, Central Clinical School, Sydney Bioinformatics, University of Sydney, Sydney, NSW, Australia

Introduction

L-Tryptophan is an amino acid containing an indole nucleus incorporated into its side chain. It is the least abundant of the essential amino acids, accounting for only 1% of the total amino acid content in humans. The kynurenine pathway was first described as a major route for metabolism of tryptophan in 1947 (Beadle et al. 1947) and was of interest both as a source of nicotinamide and as the first metabolic pathway affected by the onset of vitamin B6 deficiency.

The first step of the kynurenine pathway is the oxidative cleavage of the 2,3-double bond of the indole ring of L-tryptophan, *via* the incorporation of molecular oxygen or

a superoxide anion. The heme-containing enzymes tryptophan 2,3-dioxygenase (TDO) and indoleamine 2,3-dioxygenase-1 (IDO1) are both capable of catalyzing this reaction. The cleavage product, *N*′-formylkynurenine, is then hydrolyzed by kynurenine formamidase or decays spontaneously to kynurenine plus formic acid. Kynurenine has a number of different metabolic fates, including the production of the neuroactive metabolites quinolinic and kynurenic acid (Fig. 1).

Although TDO and IDO1 both catalyze the first step in the kynurenine pathway, they differ in their substrate specificity and expression pattern. TDO, a tetramer with a subunit molecular weight (MW) of 103 kDa, is found predominantly in the liver (Tankiewicz et al. 2003), placenta (Suzuki et al. 2001) and brain (Haber et al. 1993) and its expression is up-regulated by glucocorticoids (Danesch et al. 1983, 1987) and dietary tryptophan (Knox 1966). Reductants such as ascorbic acid (AA) and borohydride initiate catalytic activity in vitro by reducing the inactive ferric (Fe^{3+}) form of the heme iron of IDO/TDO to the active ferrous (Fe^{2+}) form. TDO is an enantiomer-specific enzyme, only capable of cleaving the indole ring of L-tryptophan.

Indoleamine 2,3-dioxygenase-1 is present in the intestine, placenta, lung, blood mononuclear phagocytes, epididymis, endocrine glands and central nervous system (Hansen et al. 2000; Heyes and Morrison 1997; Stone et al. 2003; Suzuki et al. 2001). Numerous cell types, including dendritic cells (DCs), macrophages, fibroblasts and endothelial cells, express IDO1 in response to interferon (IFN)-α, IFN-γ, lipopolysaccharide (LPS), interleukin (IL)-1 or tumor necrosis factor (TNF) exposure. IDO1 is a monomeric, heme-containing enzyme that requires reduction of the ferric heme iron to the ferrous form for activity. Superoxide anion was long thought to be the cellular reductant of IDO1; however, recent data suggest that cytochrome b_5 is more likely to be the physiological electron donor (Maghzal et al. 2008; Vottero et al. 2006). IDO1 has a broader substrate range than TDO and is capable of cleaving the indole rings of D- and L-tryptophan, tryptamine, 5-hydroxytryptophan, 5-hydroxytryptamine and melatonin (Shimizu et al. 1978; Thomas and Stocker 1999).

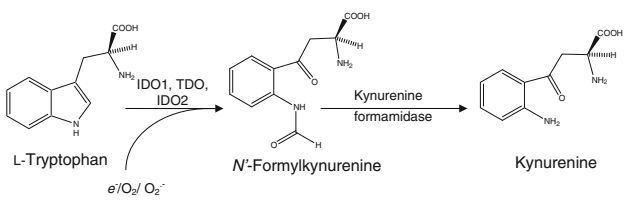

Fig. 1 Initial steps of the kynurenine pathway

High levels of IDO1 activity can lead to depletion of tryptophan in the cellular environment. This may slow cellular and microbial growth (Pfefferkorn et al. 1986) or have immune regulatory effects, such as inducing apoptosis in T cells (Fallarino et al. 2002; Williams et al. 2007). The inhibition of T cell responses by IDO1 activity is involved in pregnancy (Honig et al. 2004), cancer (Frey and Monu 2008) and allergy (Novak 2006). IDO1 expression and the increased production of down-stream metabolites of kynurenine is associated with several central nervous system disorders, including AIDS dementia complex (Heyes et al. 1992a, b), Alzheimer's disease (Heyes et al. 1992a, b) and cerebral malaria (Hansen et al. 2004; Hunt et al. 2006).

Recently, a paralog of human and mouse IDO1 was discovered and named indoleamine 2,3-dioxygenase-2 (IDO2) (Ball et al. 2007; Metz et al. 2007; Yuasa et al. 2007). In mice and humans, the IDO1 and IDO2 genes have a similar genomic structure and are situated adjacent to each other on chromosome 8, suggesting that they arose by a gene duplication event. The IDO1 and IDO2 proteins, both human and mouse, have 43% similarity at the amino acid level. IDO2 is primarily expressed in the murine kidney, reproductive tract and liver and its expression does not change in murine malaria, a disease with high circulating levels of cytokines (Ball et al. 2009). While IDO2 was demonstrated to catalyze the first step in the kynurenine pathway, a physiological role for the enzyme has not yet been discovered. Metz et al. (2007) reported that 1-methyl-D-tryptophan (1-MDT) was a preferential inhibitor of IDO2 over IDO1 when expressed in T-REx cells. IDO activity in the DCs residing in tumor draining lymph nodes is thought to allow tumors to evade an immune response (Frey and Monu 2008). IDO inhibition with 1-MDT was found to be an effective chemotherapeutic agent in mouse tumor models (Hou et al. 2007), but it is yet to be demonstrated that IDO2 is involved in immune regulation.

Selective inhibitor compounds will be useful for determining the physiological role of IDO2, but no dissociation constants thus far have been described for existing compounds. The biochemical characterization of IDO2 has been hindered by lack of an in vitro assay, as IDO2 shows little activity in the assay commonly used to measure IDO1 activity (Ball et al. 2007, 2009; Yuasa et al. 2007), which employs methylene blue (MB) as the electron source. Here, we present kinetic data demonstrating that cytochrome b_5 is capable of reducing recombinant mouse IDO2 (rmIDO2) and improves its in vitro activity compared to that observed in the MB assay. We also describe the kinetics of rmIDO2 inhibition by known competitive and non-competitive IDO1 inhibitors, and the enzyme's pH stability, thermal stability and structural features. The data show that IDO1 and IDO2 have very different biochemical characteristics

despite similar predicted tertiary structures, suggesting distinct physiological functions.

Experimental procedures

Unless otherwise stated, all reagents were obtained from Sigma-Aldrich.

Expression constructs for rmIDO1 and rmIDO2

Cloning and construction of the mouse IDO1 expression vector was performed as outlined earlier (Austin et al. 2009) and sub-cloning of the mouse IDO2 cDNA (pENTR-mIDO2) as previously described (Ball et al. 2007). The cDNA was recombined into pDEST17 using LR-recombinase according to the manufacturer's instructions (Invitrogen). A Factor Xa cleavage site was engineered into a pDEST17-rmIDO2 construct to allow for the release of rmIDO2 from the 6-His fusion partner for use in experiments to verify that the His tag did not influence the characteristics of expressed IDO2. For sequences of rmIDO2 constructs see Supplementary Materials.

Expression of rmIDO2

Cultures of transformed KRX cells (Promega) were grown in 1 L of Terrific Broth (TB) medium containing carbenicillin (50 mg/mL) at 37°C until an $OD_{600\ nm}$ of 0.8 was reached. The cultures were then grown at room temperature to an $OD_{600\ nm}$ between 1.0 and 1.5. Isopropyl β-D-1-thiogalactopyranoside (IPTG), rhamnose (20% w/v) and δ-aminolevulinic acid hydrochloride (ALA-HCl) were added to final concentrations of 1 mM, 0.1% (w/v) and 0.5 mM, respectively (Austin et al. 2009), and the cultures were grown overnight. Cells were collected as a pellet by centrifugation at 8,000×*g* for 15 min and re-suspended in 25 mM Tris buffer pH 7.4, containing 150 mM NaCl. Concentrations of rhamnose were varied at the time of induction stage between 0.05% (w/v) and 0.1% (w/v) (recommended maximum) to optimize expression. The growth trials were performed in 500 mL TB medium or Luria–Bertani (LB) media.

Expression of rmIDO1

Escherichia coli Rosetta cells were transformed with the pDEST 17-rmIDO1 plasmid. Cultures of transformed cells were grown in 1 L of LB medium containing carbenicillin (50 mg/mL) and chloramphenicol (35 mg/mL) at room temperature until an $OD_{600\ nm}$ between 0.3 and 0.4 was reached. IPTG and ALA-HCl were then added to final concentrations of 0.025 and 0.5 mM, respectively, and the cultures were grown overnight. Cells were collected as a pellet by centrifugation at 8,000×*g* for 15 min and re-suspended in 25 mM Tris buffer pH 7.4, containing 150 mM NaCl. Purification of rmIDO1 was carried out as described for rmIDO2.

Purification of rmIDO1 and rmIDO2

One liter pellets of bacterial culture were re-suspended in 25 mM Tris–HCl (pH 7.4), containing 150 mM NaCl, 10 mM imidazole, 10 mM $MgCl_2$, lysozyme (1 mg/mL), EDTA-free cocktail inhibitor tablets (2×), DNase (<1 mg) and 1 mM phenylmethylsulphonyl fluoride (PMSF). The re-suspended bacterial pellet was incubated on ice for 1 h. The suspension was sonicated (Branson Sonifier, 3 × 40 W, 30 s pulses) before centrifugation at 5,000×*g* for 20 min to obtain a clear supernatant.

The supernatant (25 mL) was applied to a 1 mL Hi-Trap chelating column (Amersham Biosciences) that had been charged with nickel ions and equilibrated with the basal buffer [25 mM Tris–HCl (pH 7.4), 150 mM NaCl, 1 mM PMSF, 10 mM imidazole]. Following washing with 18 mL of basal buffer, recombinant enzyme was eluted on a gradient from 10 to 300 mM imidazole. Fractions with high $A_{406\ nm}$:$A_{280\ nm}$ ratio were pooled, buffer-exchanged into 50 mM Tris (pH 7.4) using an Amicon Ultra (Millipore) 4 mL centrifugal device with a 30,000 Da molecular weight cut-off, then diluted with a 1:1 addition of 80% glycerol for storage at −80°C.

Protein concentration was determined with Bio-Rad® dye reagent (1:5 Dilution with MilliQ H_2O), using bovine serum albumin (0–1 mg/mL) as a standard. The colored product was measured at 595 nm using a SpectraMax 190 micro-plate reader.

The fusion protein was cleaved by Factor Xa protease (Qiagen Co.) according to the manufacturer's instructions. Briefly, purified rmIDO2 was concentrated and re-suspended in ice-cold reaction buffer (20 mM Tris–HCl, pH 6.5; 50 mM NaCl; 1 mM $CaCl_2$) and the aliquot was treated with Factor Xa protease (12.5 U/mL) for 2 h at 4°C. Factor Xa protease was removed through application of Factor Xa Removal Resin (Qiagen) and the liberated rmIDO2 separated from undigested His-tagged protein by application of the aliquot to a Hi-Trap chelating column equilibrated with reaction buffer.

Biochemical assays

Recombinant proteins were typically added to reaction mixtures at dilutions of 1:100–1:2,000 depending on the stock concentration and reactivity of the enzyme. Final glycerol concentrations in working solutions were less than 0.4% (v/v). Tryptophan catabolizing activity initially was

determined by the MB/AA assay as described by Takikawa et al. (1988) and elsewhere (Austin et al. 2009) with minor modifications.

Using the MB assay, the kinetic properties of rmIDO2 and rmIDO1 were determined against three substrates, i.e. L-tryptophan (0–40 mM), D-tryptophan (0–200 mM) and 5-hydroxy-L-tryptophan (0–150 mM). Each reaction was conducted in triplicate. Kinetic parameters (K_m, V_{max}, and standard error) were determined using GraphPad Prism 4.

For hypoxanthine/xanthine oxidase activity assays, rmIDO2 (100 nM in heme) in 50 mM potassium phosphate buffer pH 7.4, 200 μg/mL catalase, and 50 μM diethylene triamine pentaacetic acid (DTPA) was incubated for 30 min at 37°C with 2 mM L-Trp, 100 μM hypoxanthine, and varying concentrations of xanthine oxidase. The rate of $O_2^{\cdot-}$ generation was determined by the rate of reduction of ferric cytochrome *c*. In 50 mM phosphate buffer pH 7.4, 240 μg horse heart cytochrome *c* was mixed with 615 U bovine catalase, 50 μM DTPA, and varying concentrations of xanthine oxidase. Reaction mixtures were incubated at 37°C for 10 min before addition of 100 μM hypoxanthine, and $OD_{550\ nm}$ was then monitored for 5 min at 37°C. The rate of $O_2^{\cdot-}$ production was calculated using an extinction coefficient of $21.1 \times 10^3\ M^{-1}\ cm^{-1}$.

For the cytochrome b_5 (cyb_5)/cytochrome P450 reductase (CPR) cofactor assay of IDO1 and IDO2 activity, the standard reaction mixture was similar to Maghzal and colleagues with minor modifications (Maghzal et al. 2008).

Molecular techniques

SDS-PAGE was performed according to the method of Laemmli (1970) using a Bio-Rad Mini-Protean III system. Western blotting was performed according to the methods outlined elsewhere (Ball et al. 2007).

Protein structure prediction

The structures of mouse IDO2 and mouse cyb_5 were predicted using SWISS-MODEL (Peitsch 1995), via the web interface of Swiss-PdbViewer. Suitable template structures were selected based on their sequence similarity. The structure of mIDO2 was modeled on the crystal structure of IDO1 (PDB: 2D0T:A, E value $= 1e^{-100}$, sequence identity = 43%, resolution = 2.3 Å). The structure of mouse cyb_5 was based on the NMR structure of rat cyb_5 (PDB: 1JEX:A, E value $= 2e^{-139}$, sequence identity = 89%). After the project was submitted to SWISS-MODEL, optimization was carried out by the GROMOS96-forcefield (van Gunsteren et al. 1996).

Models of association of mIDO2 with mouse cyb_5 were generated by the fully automatic ClusPro protein–protein docking server (Comeau et al. 2004). Rigid body docking was performed, using ZDOCK (Chen et al. 2003). ZDOCK uses a fast Fourier transform method to rapidly search for low-energy configurations based on shape complementarities, electrostatic potentials, and desolvation terms. The ZDOCK searches were conducted at 6° orientational steps and the final 2,000 configurations subjected to clustering analysis yielding ten final receptor-ligand complexes. In addition, the structural models of mIDO2 and cyb_5 were entered independently into the RosettaDock protein–protein docking server (Lyskov and Gray 2008).

Comparison of K_i values for competitive and non-competitive inhibitors

For inhibitor testing, known inhibitors of IDO1 (competitive: 1-methyl-L-tryptophan (1-MLT) and 1-MDT; non-competitive: norharman) were added to the standard reaction mixture (outlined above) over a concentration range with carrier controls. L-Tryptophan substrate concentration was also varied over a concentration range, with carrier controls. K_i values were determined *via* non-linear regression analysis using GraphPad Prism 4. The following non-linear regression equations were used: non-competitive, $Y = [V_{max}X/(1 + I/K_i)]/K_m + X$; and competitive, $K_m(app) = K_m[1 + I/K]$, $Y = V_{max}X/[K_m(app) + X]$.

Circular dichroism

Circular dichroism (CD) spectra were recorded on a JASCO J-810 spectropolarimeter with 1 mm path length quartz cuvettes at a temperature of 20°C. Sensitivity was 100 millidegrees, and the scanning speed was 50 nm/min for an accumulation of 32 scans. CD data were collected between 300 and 190 nm. Data collected in this region were further analyzed using SOMCD, the neural network algorithm (Unneberg et al. 2001). Thermal transition curves were measured by monitoring $\lambda = 222$ nm as a function of the increasing temperature over the range 20–99°C at 1 °C/min. T_m values were determined by finding the first derivative of the thermal transition curve using peak processing software packaged with the JASCO J-810 spectropolarimeter.

Determination of pH and salt profiles

The pH stability test was carried out in a standard reaction mixture containing 100 mM potassium phosphate buffer, 100 mM KCl. The pH was varied in increments of 0.2 pH units within a range of pH 6–9. For salt stability tests the standard reaction mixture contained 100 mM potassium phosphate buffer, pH 7.4, with salt concentrations ranging from 0 to 300 mM. For pH and salt profiles, the

L-tryptophan concentration was kept constant for rmIDO1 (400 μM) and rmIDO2 (30 mM).

UV–visible spectroscopy

Optical absorption spectra of rmIDO1 and rmIDO2 (10–15 μM in heme) were recorded in 100 mM potassium phosphate buffer (pH 7.5) degassed with argon in a SpectraMax 190 micro-plate reader. Ferrous iron (Fe^{2+}) rhIDO1 was formed by the addition of a molar excess of a buffered sodium dithionite solution. Nitric oxide (NO) was introduced by direct addition of 2 mM solution of diethylamine NONOate (DEANO) in deoxygenated phosphate buffer (pH 7.5). RmIDO1 and rmIDO2 spectra were gathered immediately after addition of sodium dithionite or sodium dithionite and DEANO.

Reduction of rmIDO2 by cytochrome b_5

The reduction of rmIDO2 by recombinant human cytochrome b_5 was investigated by adding 8 μM Fe^{3+}–rmIDO2 to a reaction mixture purged with argon gas and containing 0.2 μM human recombinant cytochrome b_5, 2 μM purified human NADPH:CPR, 56 U glucose-6-phosphate dehydrogenase, 375 U bovine catalase, 20 mM glucose-6-phosphate, 4 mM $NADP^+$, and 200 μM DTPA acid in 100 mM phosphate buffer, pH 7.4. The reaction was carried out at 25°C in a septum-sealed cuvette thoroughly purged with argon gas. Difference spectra were recorded every 30 s from 350 to 750 nm against a reference sample containing the reaction mixture without rhIDO, using a Beckman-Coulter DU800A spectrophotometer. Solutions of glucose-6-phosphate dehydrogenase and NADPH:CPR were gel-filtered prior to use to remove any interfering substances such as ammonium sulfate and dithiothreitol.

Results and discussion

The discovery of a third enzyme capable of catalyzing the cleavage of L-tryptophan adds a new dimension to the important role played by the kynurenine pathway in physiological processes including innate immunity. Characterization of rmIDO2 through the comparison of kinetic and structural features to human and mouse IDO1 helps to define a new target for pharmacological intervention.

Expression, purification and characterization

The heterologous over-expression of rmIDO2 protein was optimized using KRX cells. The best expression conditions were obtained using TB medium and induction with a final concentration of 0.1% (w/v) rhamnose. The expression system was supplemented with ALA, a natural precursor of heme, in order to increase the heme content as reported for IDO1 (Austin et al. 2004) and other heme proteins (Delcarte et al. 2003). Purification of the protein over a Ni-NTA column yielded 7.5 mg/L of cell culture. Only one band was observed by SDS-PAGE for both isolated proteins with a molecular mass of ~45 kDa. pDEST17 clones, including recombinant IDO enzymes investigated in this study, contain a 3.2 kDa N-terminal addition to allow for expression of the 6-His tag. Theoretical molecular weights for rmIDO1 and rmIDO2 are therefore 45.3 and 45.2 kDa, respectively.

Expression of rmIDO2 was demonstrated by Western Blot analysis with both mIDO2 and His tag antibodies. A specific band of predicted size for rmIDO2 (~45 kDa) was observed (Supplementary Data). Comparison between the biochemical activities of His-tag cleaved and non-cleaved rmIDO-2 indicated that the addition of the 6-His tag had little effect on kynurenine production (Supplementary Data).

Circular dichroism

Circular dichroism spectra were acquired to compare the gross secondary structure of rmIDO1 and rmIDO2 (Fig. 2a). Far UV CD spectra were analyzed using SOMCD (Table 1). Analysis showed that both enzymes are predominantly α-helical, 71 and 75% for rmIDO1 and rmIDO2, respectively. RmIDO2 had a higher percentage of random coil, 16%, as opposed to 10% in rmIDO1. Despite these small differences, the secondary structures of both mouse enzymes were broadly similar to each other as well as the observed secondary structure elucidated from the crystal structure of human IDO1 (61% α-helix, 1% β-sheet) (Sugimoto et al. 2006).

Stability data: thermal and pH

While secondary structure and the heme environment of rmIDO2 are similar to rmIDO1 and hIDO1, distinctions in both pH and thermal stability were observed. Thermal denaturations of rmIDO1 and rmIDO2 were observed using CD spectrometry. Loss in structure was monitored at $\lambda = 222$ nm (Fig. 2b). The T_m of the denaturation process for rmIDO1 was 60°C, with a possible second intermediate at a T_m of 48°C. RmIDO2 denatured in a single step, with a T_m at 48°C. The optimum activity of rmIDO1 occurred at pH 6.0–6.5, whereas rmIDO2 was most active at pH 7.4–7.5 (Fig. 3). Tests with various buffers showed that 100 mM potassium phosphate pH 7.5 was a suitable buffer for rmIDO2 in the MB assay and was therefore used for further analysis.

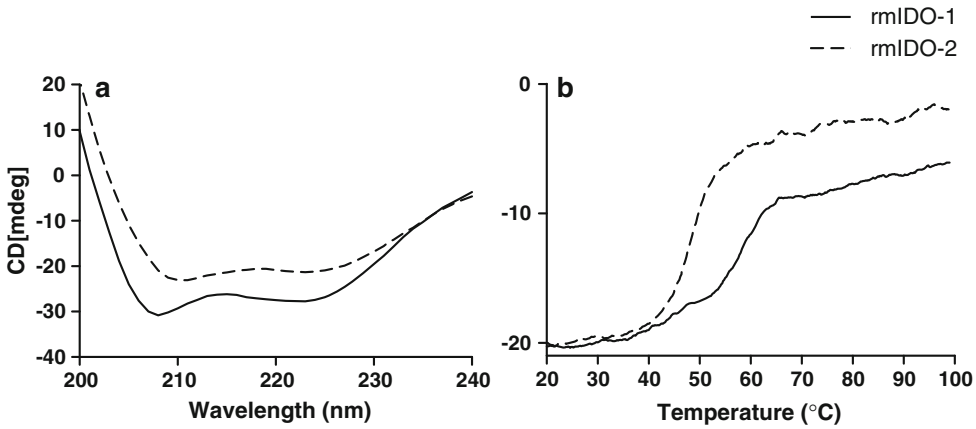

Fig. 2 **a** Circular dichroism analyses of rmIDO1 and rmIDO2. **b** Thermal transition of rmIDO1 and rmIDO2 at $\lambda = 222$ nm over the range 20–99°C. Circular dichroism spectra were obtained in 10 mM Tris (pH 7.4) buffer with a 1 mm pathlength cuvette. Protein concentration: 1 mg/mL

Table 1 Secondary structure analyses of rmIDO1 and rmIDO2 by circular dichroism

Protein	rmIDO1 (%)	rmIDO2 (%)
α-Helix	71	75
β-Sheet	4	3
β-Turn	15	6
Random coil	10	16

Localization in vivo may be a factor in thermal/pH enzyme stability. For example, IDO2 is present in sperm tails (Ball et al. 2007), and sperm synthesis in the testis occurs at a significantly colder (~2°C) temperature than core body temperature (Harrison and Weiner 1949). Seminiferous fluid has a normal pH of 7.2–8.0 (World Health Organization. 1999), consistent with the observed optimal pH range for IDO2 activity (Fig. 3).

Proximal and distal tubules of the kidney are responsible for amino acid filtration from plasma; as a result of this high volume throughput, amino acid levels found in the kidney tubules can be much higher than plasma (Silbernagl 1988). With a high capacity for substrate, constitutive expression (Ball et al. 2007) and optimum activity within the physiological plasma pH range, IDO2 may metabolise L-tryptophan taken up from the renal filtrate.

Structure prediction

Given the similar secondary structures and 43% sequence identity between mouse IDO2 and human IDO1, the crystal structure of human IDO1 described by Sugimoto et al. (2006) was considered an appropriate scaffold for predicting the structure of mouse IDO2. To better visualize some of the similarities and differences in the heme environment and secondary structure of hIDO1, mIDO1 and mIDO2, we used spectroscopic studies to probe the heme site and structure prediction software to model the 3D structure of mIDO2.

The large predicted domain of mouse IDO2 consists of 13 α-helices and two 3_{10} helices. The smaller predicted domain of mouse IDO2 is comprised of six α-helices, two short β-sheets and three 3_{10} helices (Fig. 4). A comparison of the amino acids 360–380 is not possible as disordered electron density prevented resolution of this region of the enzyme in the Sugimoto et al. (2006) crystal structure.

There is a high degree of amino acid conservation in the heme-binding sites of hIDO1 and mIDO2. However, substrate access to the heme in mIDO2 (Fig. 4a) appears to be decreased in comparison to hIDO1 (Fig. 4b) due to steric hindrance by bulky amino acids at the entrance to the 'pore'. Specifically, substitution of the human IDO1 I217 and L384 with methionine (mIDO2: M221 and M385, respectively—Fig. 4c, d) may result in a reinforcement of

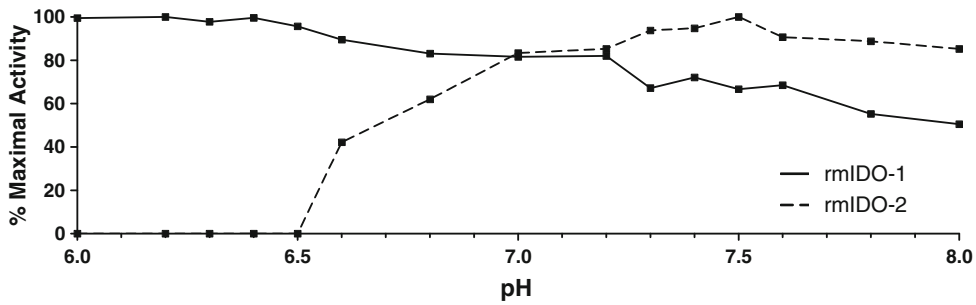

Fig. 3 Effect of pH on percentage of maximum enzyme activity. RmIDO1 had a global maximum at pH 6.0–6.5; rmIDO2 had a global maximum at pH 7.5

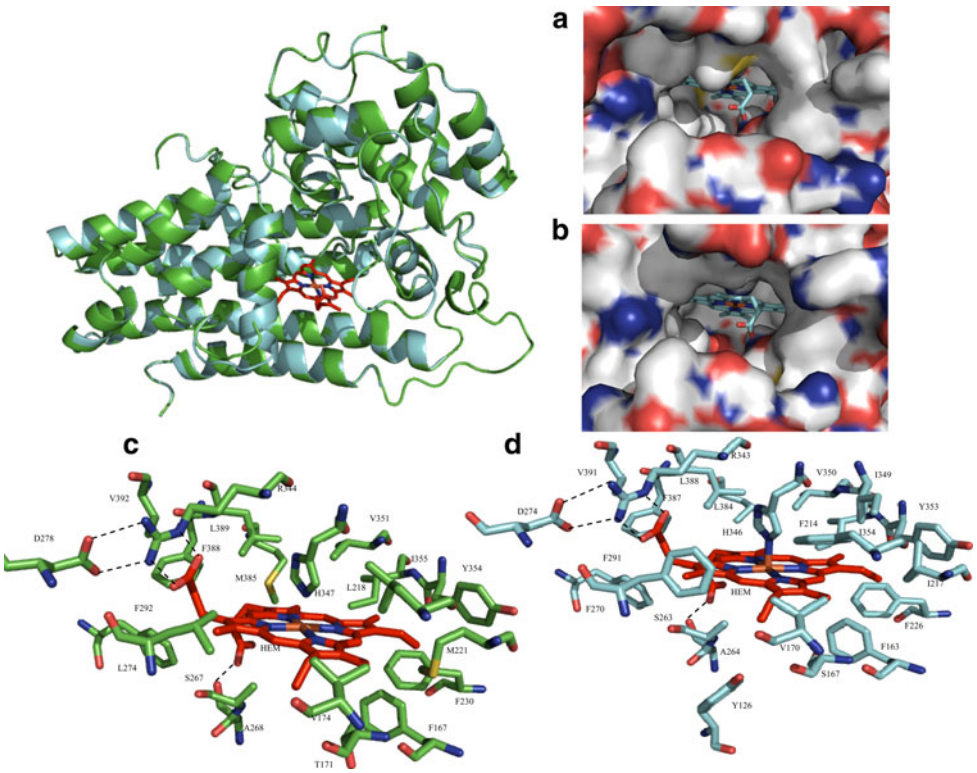

Fig. 4 Superimposed structures of rhIDO1 (PDB-ID: 2D0T) and rmIDO2. Residues superimposed were obtained from pairwise sequence alignment. RhIDO1 is *blue* and rmIDO2 is *green*. There is a gap in PDB data for rhIDO1 between the amino acids 360–380. **a** Substrate access to heme moiety in rmIDO2. **b** Substrate access to heme moiety in rhIDO1; negative charges (*red*), positive charges (*blue*), sulfur atoms (*yellow*). **c** Amino acids within 4 Å of the heme in mIDO2 (except D278). **d** Amino acids within 4 Å of the heme in hIDO1 (except D274)

heme binding (Kurokawa et al. 2004) or a change in the oxidation state of heme (Kim et al. 2001). As indicated by the predicted three-dimensional structure of mouse IDO2, this methionine might be responsible for differences in accessibility of the heme-binding site, substrate binding and catalytic activity between mIDO2 and mIDO1.

Three amino acids (F226, F227 and R231) were deemed critical to maintaining dioxygenase activity in IDO1 (Sugimoto et al. 2006). Forming part of the entrance to the heme-binding pocket, these residues are involved in substrate recognition through hydrophobic F226, F227 and R231 interactions (Figs. 4, 5). Two of the three amino acids are conserved in mouse IDO2, namely F230 (corresponding to F226 in human IDO1) and R235 (corresponding to F231 in human IDO1). F227 (human IDO1) has undergone a substitution to Y231 (mouse IDO2). While a phenylalanine–tyrosine mutation is considered conservative, in terms of amino acid structure and degree of nucleotide change, this mutation may make the heme-binding pocket of mIDO2 more susceptible to phosphorylation (Calalb et al. 1995) or sulfation (Kehoe and Bertozzi 2000). Reduced substrate activity in IDO2 may be due to post-translational modification not experienced by IDO1.

Spectral characteristics

The Soret band for heme proteins is typically observed in the near-ultraviolet region at approximately 400 nm. Alteration of the porphyrin chromophore *via* reduction or ligand binding produces shifts in the visible spectrum that can offer valuable comparative data. Proteins containing high spin heme species typically absorb in the 400–410 nm region, while low spin species absorb above 410 nm. In the α/β region, low spin ferric species give two prominent bands, whereas high spin species have more complex spectral features.

RmIDO2, like rmIDO1, is a ferric (Fe^{3+}) type heme protein. Under oxidized conditions, rmIDO1 and rmIDO2 both displayed similar γ-Soret peaks at 406 nm (Fig. 6a) and double peaks in the α/β region (albeit at different wavelengths—rmIDO1: 540 and 575 nm; rmIDO2: 538 and 585 nm; Fig. 6b). This mixed spin character is similar to human IDO1 and some mammalian globins (Feis et al. 1994; Terentis et al. 2002).

The spectrum of Fe^{2+} rmIDO1 and rmIDO2 provides structural information on the catalytically active enzyme (Fig. 6). Dithionite-reduced rmIDO1 and rmDO-2 (Fe^{2+}) both displayed γ-Soret bands at 428 nm (Fig. 6a) and broad α/β peaks at around 555–560 nm (Fig. 6b). Again, both enzymes displayed similar absorbance spectra; reduction altered the heme into a high spin-state as indicated by the red shift in the Soret peak and broadening of peaks in the α/β region.

We also examined interactions with NO (Fig. 6), a known inhibitor of rhIDO1, to assess changes in the heme environment of catalytically active rmIDO2. A bolus

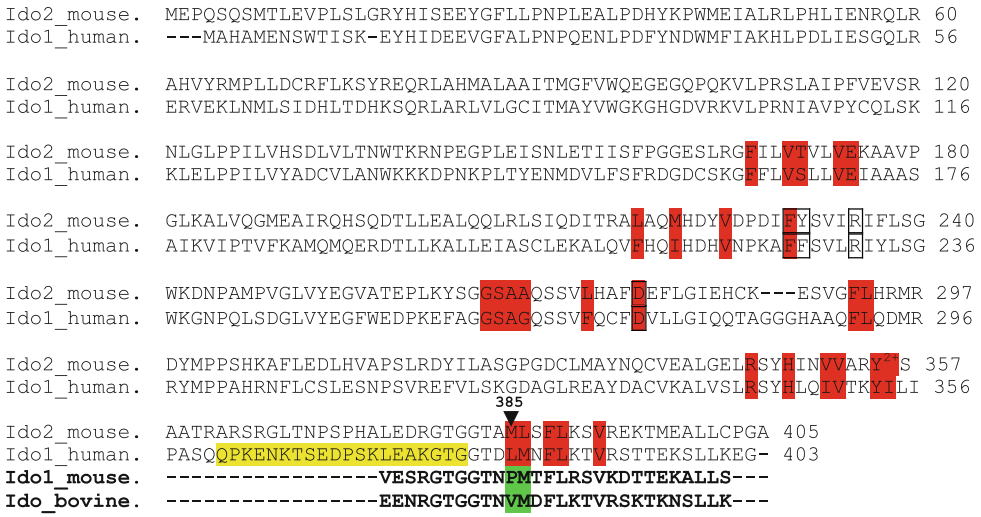

Fig. 5 Alignment of the amino acid sequences of human IDO1 and mouse IDO2. Sequence identity: 43%. Amino acids *highlighted in red* interact with the heme molecule. *Yellow* region could not be modeled because of the disordered electron density. *Outlined* amino acids are those that are most likely involved in substrate recognition by hydrophobic interactions (Sugimoto et al. 2006). *Bold alignment* sequence alignment of active site residues of two mammalian IDO1 enzymes. Methionine 385 of mouse IDO2 has a prominent alternative position to other IDO enzymes (as indicated by *arrow* and *green highlighting*)

addition of 2 mM DEANO resulted in a large red shift of the Soret γ band maximum for both enzymes, the appearance of two distinct bands in the α/β region for rmIDO2, and a small blue shift for the existing α/β peaks in rmIDO1 (Fig. 6c, d). Under both oxidized and reduced conditions, rmIDO1 and rmIDO2 displayed low spin absorbance characteristics, indicative of direct binding of NO to form an iron-complex independent of the redox state, similar to rhIDO1 (Thomas et al. 2007). This suggests that NO could potentially also inhibit IDO2 activity. The addition of DEANO to Fe^{2+} rmIDO1 and rmIDO2 resulted in a shift of the γ-Soret band to 418 and 419 nm, respectively (Fig. 6e). The appearance of peaks in the α/β region at 545 and 575 nm was observed in both enzymes (Fig. 6f).

Kinetic activity

In the MB/AA assay, for the major IDO1 substrate L-tryptophan, the K_m of rmIDO2 was 430 times higher than that of rmIDO1, with little evidence of the substrate inhibition that becomes apparent with IDO1 at high tryptophan concentrations (20–40 mM). Despite the high tryptophan concentrations, the V_{max} of the enzyme remained low (Table 3). Differences in the reduction potentials of mIDO1 and mIDO2 may account for the disparate behavior in the presence of MB/AA.

There is also a discrepancy between the in vivo and in vitro kinetic activity of the enzyme. We reported that rmIDO2 generated 45% less kynurenine than rmIDO1 when the two proteins were expressed at similar levels in intact mammalian cells (Ball et al. 2007). Clearly, the current IDO1 in vitro assay system utilizing MB/AA is inadequate for optimal IDO2 activity.

We replaced MB/AA with hypoxanthine and xanthine oxidase, a well-established enzymatic system to generate $O_2^{\cdot-}$ (Fig. 7). We chose the concentrations of hypoxanthine and xanthine oxidase such that the amounts of $O_2^{\cdot-}$ generated would be in molar excess when compared to rmIDO2 levels. The result obtained show that while $O_2^{\cdot-}$ can activate isolated rmIDO2, the extent of this activation is modest, yielding levels of activity similar to the MB/AA system.

Recently it has been shown that cyb_5, not the superoxide anion radical, is a major reductant of human IDO1 in cells (Maghzal et al. 2008). We hypothesized that cyb_5 acts in a similar way with mouse IDO2. To test whether cyb_5 can reduce rmIDO2–Fe^{3+}, we monitored the spectral changes to rmIDO2–Fe^{3+} in the presence of recombinant human cyb_5, CPR and an NADPH-regenerating system under anaerobic conditions (Fig. 8). Using UV–visible absorption spectroscopy, difference spectra showed a time-dependent decrease in absorbance at ~406 nm (γ-Soret band) and the appearance of a peak at ~420 nm. In addition, appearance of distinct α/β bands at 542 and 577 nm was observed concomitantly with a decrease in absorbance at 510 and 620 nm (Table 2).

The addition of human cyb_5/CPR to rmIDO2 in the presence of NADPH resulted in spectral changes similar to those reported for rhIDO1 (Maghzal et al. 2008) and methemoglobin (Kuma 1981) (Fig. 8). These results provide direct evidence that the cyb_5/CPR system can reduce rmIDO2.

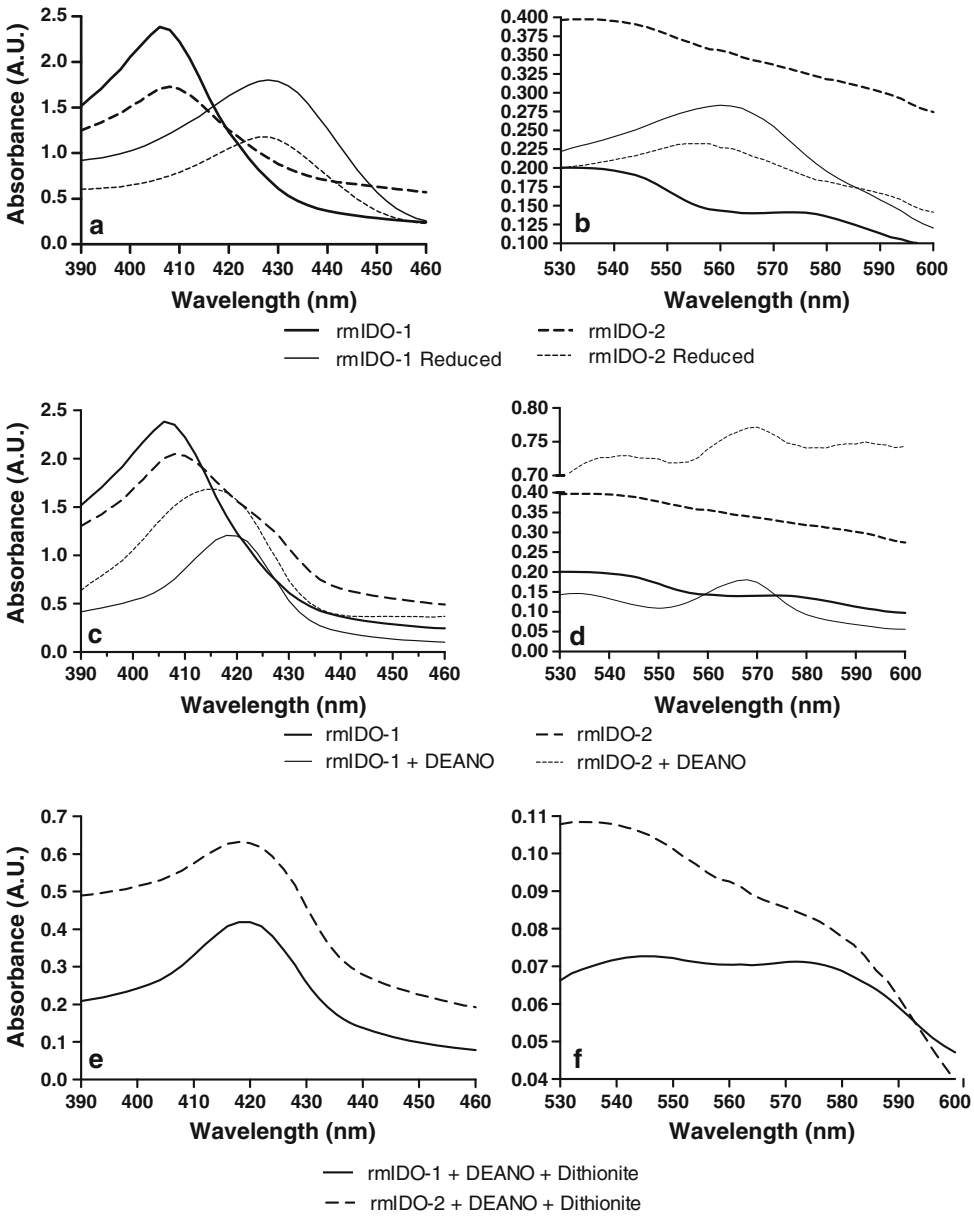

Fig. 6 Characterization of NO-inhibited rmIDO1 and rmIDO2. Ferric and Ferrous rmIDO1 and rmIDO2: **a** Soret γ region, **b** α/β region. Ferric rmIDO1 and rmIDO2 incubated in the presence of DEANO: **c** Soret γ region, **d** α/β region. Ferrous rmIDO1 and rmIDO2 in the presence of DEANO: **e** Soret γ region, **f** α/β region

In vitro assays of rmIDO2 activity incorporating cyb_5/CPR were conducted. Recombinant human cyb_5 effectively activated rmIDO2 in the presence of purified human CPR and an NADPH-regenerating system (Table 3). CPR is a physiological electron donor of cyb_5 (Schenkman and Jansson 2003), and has been used previously in vitro (Maghzal et al. 2008). The presence of both cyb_5 and CPR was required for this activity, as either protein alone failed to activate rmIDO1 or rmIDO2, even in the presence of NADPH (data not shown).

RmIDO2 showed a significant decrease in K_m and an increase in V_{max} when incubated at 37°C in the presence of an equimolar ratio of cyb_5/CPR. The K_m of rmIDO2 in the presence of cyb_5/CPR was decreased 20-fold (from 12,000 to 580 μM) over the MB/AA assay. The V_{max} of rmIDO2 was increased 4.5-fold in the cyb_5/CPR assay, from 0.027 to 0.13 μmoles/(min mg) of protein (Table 3). For experiments with rmIDO1 in the presence of cyb_5/CPR we observed a significant decrease in the kynurenine turnover of the enzyme (from 3.38 to 0.12 μmoles/(min mg) of protein). The substrate affinity of rmIDO1 for L-tryptophan remained the same. A drop in V_{max} whilst K_m remains stable is indicative of non-competitive inhibition. This implies that cyb_5 interacts with rmIDO1 not through direct competition with the substrate-binding site, but *via* another mechanism (e.g. protein–protein structural changes). This mechanism appears to be similar for both rmIDO1 and rmIDO2 as substrate turnover in the presence of cyb_5/CPR is similar.

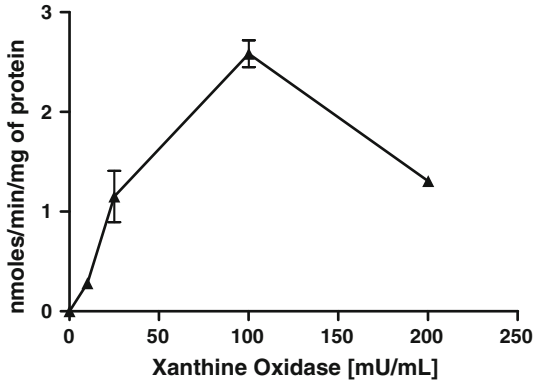

Fig. 7 Activation of rmIDO2 by xanthine oxidase/hypoxanthine. Reaction mixtures were incubated at 37°C for 1 h in the presence of 100 μM hypoxanthine. O_2^- production was confirmed by rate of reduction of ferric cytochrome using $\varepsilon_{550\ nm} = 21.1 \times 10^3\ M^{-1}\ cm^{-1}$

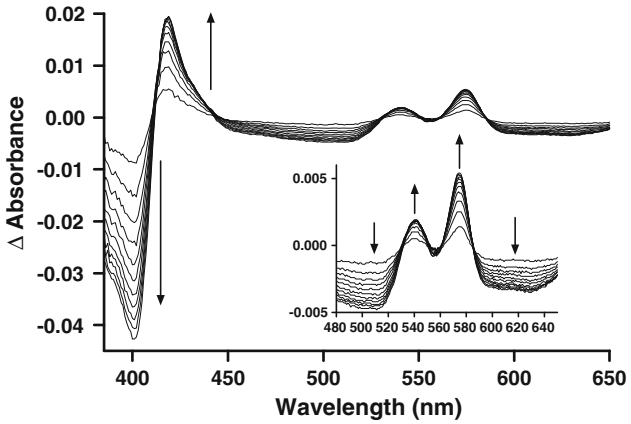

Fig. 8 Reduction of rmIDO2–Fe^{3+} by cytochrome *b*5 in the absence of oxygen. Spectra shown between 380 and 650 nm. *Inset* shows α/β region between 480 and 650 nm. *Up arrow* and *down arrow* indicate increases and decreases in absorbance over time, respectively

Table 2 Optical properties of ferric and ferrous NO complexes of rmIDO1 and rmIDO2

IDO adduct	Soret γ band	α/β Bands
rmIDO1–Fe^{3+}	406	540, 575
rmIDO1–Fe^{3+}–NO	418	532, 567
rmIDO1–Fe^{2+}	428	~560
rmIDO1–Fe^{2+}–NO	419	545, 575
rmIDO2–Fe^{3+}	406	538, 585 (shoulder)
rmIDO2–Fe^{3+}–NO	415	~540, 570
rmIDO2–Fe^{2+}	428	~555
rmIDO2–Fe^{2+}–NO	419	545, 575

Other known substrates of IDO1 were tested with rmIDO2 in both the MB/AA and Cyb_5/CPR assay. With the MB/AA assay, D-tryptophan and 5-hydroxy-L-tryptophan were turned over by nanomolar rmIDO2 concentrations in the presence of high millimolar concentrations of substrate (>150 mM) (data not shown). The possibility of contamination by L-tryptophan in preparations of alternate substrates represents a significant potential complication at such high concentrations, so these data have not been included here. Smaller indoles, tryptamine and serotonin, were also trialled as alternative substrates in the cyb_5/CPR assay. However, no significant metabolism of either molecule was observed.

Both human IDO1 and mouse IDO1 show an obvious affinity for the artificial reducing system of MB/AA. As previously demonstrated (Maghzal et al. 2008), the MB/AA assay is an efficient but inaccurate representation of IDO1 enzyme activity in vivo. RmIDO2, however, showed extremely low L-tryptophan metabolising activity in the presence of MB/AA. Cytochrome b_5 in vitro induced entirely different behaviors in these two related enzymes. Addition of cyb_5 to a reaction mixture containing rmIDO1 results in a reduction in turnover rate of IDO1 for L-tryptophan. A drop in V_{max} whilst K_m remains stable is indicative of non-competitive inhibition. However, in the case of rmIDO2 the presence of cyb_5 increased both substrate affinity and turnover rate of product. The final turnover rate in the presence of cyb_5 for both rmIDO1 and rmIDO2 was similar; indicating the possibility that, in vivo, kynurenine production by both enzymes plays a significant physiological role. However, while product turnover is similar, substrate affinity between rmIDO1 and rmIDO2, even in the presence of cyb_5, remains significantly different (Table 3; K_i 29 vs. 530 μM, respectively).

There are several distinct mechanisms through which the cyb_5/CPR system may act as a positive modifier of IDO2 activity. The direct transfer of an electron would reduce IDO2 into its active ferrous form. Alternatively, modification of the active site *via* a two heme protein complex could increase access of substrate or decrease uncoupling time of the product. Protein–protein docking studies and electrostatic potentials of mIDO2 and cyb_5 (Fig. 9) indicated that the two proteins may be capable of forming a complex.

Protein–protein docking

Rigid body docking using ZDOCK (Chen et al. 2003) yielded ten final predicted receptor-ligand complexes. In 3 of these complexes cyb_5 interacted with the heme active site of mIDO2 (Fig. 9c). In the other predicted complexes, however, the major site of interaction was on the opposite side of the proposed active site of the IDO2 molecule (Fig. 9d). Thus, the structural models of mIDO2 and cyb_5 were entered independently into the RosettaDock protein–protein docking server. The best result obtained indicated

Table 3 Kinetic and inhibitor parameters of rmIDO1 and rmIDO2 for L-tryptophan at pH 7.4

	L-Tryptophan		1-Methyl-L-tryptophan	1-Methyl-D-Tryptophan	Norharman
	V_{max} (units/mg)	K_m (μM)	K_i (μM)	K_i (μM)	K_i (μM)
rmIDO1 (MB)	3.38 ± 0.15	28 ± 4	105 ± 30	11,300 ± 400	1,080 ± 120
rmIDO1 (cyb_5/CPR)	0.12 ± 0.01	29 ± 9	80 ± 20	No competitive inhibition	1,730 ± 570
rmIDO2 (MB)	0.027 ± 0.003	12,000 ± 3000	2,750 ± 560	No competitive inhibition	690 ± 50
rmIDO2 (cyb_5/CPR)	0.13 ± 0.01	530 ± 100	440 ± 120	No competitive inhibition	1,960 ± 340

Units are expressed as μmoles/min. For methylene blue (MB) assays, the standard reaction mixture (200 μL) contained, 20 mM AA (neutralized with NaOH), 200 μg/mL catalase, 10 μM MB, 50 nM rmIDO1 or rmIDO2 and substrate. For cyb_5/CPR assays, the standard assay mixture (200 μL) contained, 50 nM rmIDO1 or rmIDO2 and substrate in the presence of 50 nM recombinant human cytochrome *b*5 (cyb_5) and 50 nM NADPH cytochrome P450 reductase (CPR). Concentrations of other compounds were as follows: 5 mM glucose 6-phosphate (*G6P*), 2.8 units of glucose-6-phosphate dehydrogenase (*G6PDH*), 2 mM NADPH. All reactions were performed in 100 mM phosphate buffer, pH 7.4 and were performed at 37°C for 30 min. The reactions were stopped by adding trichloroacetic acid, and kynurenine was measured in the supernatants. Data are mean ± standard error of the mean (SEM)

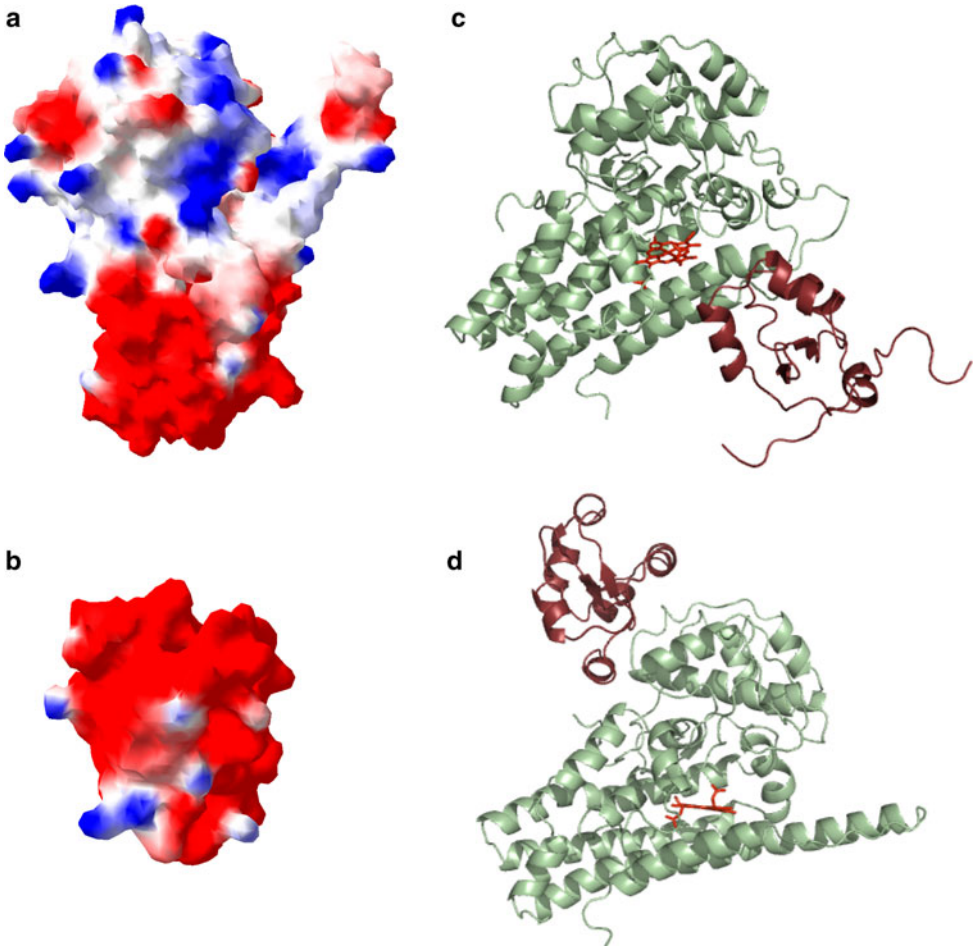

Fig. 9 Docking models of mIDO2 and cyb_5. **a** Electrostatic surface potential of mIDO2, **b** electrostatic surface potential of cyb_5. *Blue* positive potential, *red* negative, *white* neutral. **c**, **d** The protein–protein interaction site was calculated using the ClusPro and the RosettaDock protein–protein docking servers. Best energy scores were obtained for the complex shown in **d** where cyb_5 binds opposite to the heme active site. However, the complex shown in **c**, where cyb_5 directly influences the active site of the enzyme, could theoretically occur but is predicted to be less energetically favorable

binding of cyb_5 opposite the active site as shown in Fig. 9d (energy score values of 1,000 predicted complexes: −438 to −424). When the complex in which cyb_5 bound close to the mIDO2 heme active site was entered into RosettaDock, less favorable energy scores (−400 to −370) resulted. Thus, although both displayed interactions are theoretically possible, a binding opposite the heme active site is energetically favoured. Only structural models of the two molecules were available for docking analysis, and the protein–protein interaction model needs to be confirmed by mutational studies and, ideally, by X-ray crystallography. (A similar protein–protein docking study for human IDO1 and human cyb_5 was completed—yielding similar types of interactions—see Supplementary Data 4.)

Inhibitors of rmIDO2

The ability of known IDO1 inhibitors (1-MDT, 1-MLT and 1-MT) to block the activity of IDO2 in T-REx cells has been assessed previously (Metz et al. 2007). We investigated how isolated, purified rmIDO1 and rmIDO2 activity was affected by the D- or L-stereoisomers of 1MT and a known non-competitive inhibitor of IDO1, norharman (Table 3).

In the MB/AA activity assay, rmIDO1 activity was preferentially inhibited by 1-MLT (K_i 105 μM) versus 1-MDT (K_i 11.3 mM). No significant change in the K_i of 1-MLT (K_i 80 μM) against rmIDO1 was observed in the cyb_5/CPR assay. However, for 1-MDT, the addition of cyb_5/CPR resulted in a loss of inhibitory activity, albeit from very low inhibition to nil.

The stereoselectivity of the tryptophan-binding site of IDO1 has been previously investigated by Peterson et al. (1994) 1-MLT showed greater inhibition (52.3% at 100 μM inhibitor concentration) of human IDO1 than 1-MDT (5.7% inhibition at 100 μM). This observation was supported by Southan et al. (Southan et al. 1996), who showed that 6-nitro-L-tryptophan (52% inhibition at 1 mM) is an effective inhibitor of the enzyme, whilst 6-nitro-D-tryptophan showed almost no inhibitory activity (7% inhibition at 1 mM).

Inhibition of rmIDO2 activity showed a similar pattern to rmIDO1. 1-MLT was a more potent inhibitor of rmIDO2 than 1-MDT in both the MB/AA and cyb_5/CPR assays (2.75 mM and 440 μM, respectively). For 1-MDT, under these assay conditions, no inhibition of rmIDO2 activity could be observed.

We observed a similar trend for the inhibition of mIDO2 activity in transfected HEK293T cells (Supplementary Data 5). These results contrast with a previous study on the inhibitory behavior of 1-MDT against IDO2 (Metz et al. 2007). Our study found that 1-MLT was a better inhibitor of both mouse IDO1 and IDO2 using three different batches of 1-MDT and 1-MLT in three types of activity assay.

1-Methyl-D-tryptophan is efficacious as a chemotherapeutic agent in mouse tumor models (Hou et al. 2007). The report that 1-MDT was a selective inhibitor of IDO2 suggested that IDO2 was involved in immune responses to tumors (Metz et al. 2007). This was puzzling as 1-MDT was not effective in IDO1$^{-/-}$ mice, suggesting that the compound acted through IDO1 (Hou et al. 2007). The lack of mIDO2 inhibition by 1-MDT does not support its role in evasion of immune responses by tumors. However, as it is still not clear how the anti-tumor activity of 1-MDT could be mediated through IDO1, other indirect inhibitory mechanisms in vivo may need to be considered.

Norharman, a non-competitive inhibitor, based on the β-carboline structure, showed comparable levels of inhibition of rmIDO1 and rmIDO2 in the MB/AA assay, indicating a similar mode of action/binding site on both enzymes (Table 3). In the presence of cyb_5/CPR, norharman did not inhibit kynurenine production with similar potency. Non-specific interaction of norharman with cyb_5/CPR, or steric hindrance of the norharman-binding site due to interaction between proteins in the activity assay, may account for these differences in inhibitory potency.

For future experiments requiring inhibition of both IDO1 and IDO2 activity, L-stereoisomer tryptophan analogs or norharman (and related compounds) may offer the best lead compounds for testing. Further development of IDO1 or IDO2 selective inhibitors is required.

In 1989, Sono stated that "some physiological electron carrier(s) between the donor(s) and the dioxygenase might exist. Such an activation process may not require $O_2^{\cdot-}$" (Sono 1989). Since then, IDO-like proteins have been discovered with a myoglobin-like oxygen transport activity in molluscs (Suzuki et al. 1998), and cyb_5 has been shown to regulate IDO1 activity in yeast (Vottero et al. 2006) and mammalian cells (Maghzal et al. 2008). As a close evolutionary relative of both IDO1 and the gastropod myoglobins, the role cyb_5 plays in activation of rmIDO2 in vitro lends further support to the conclusions drawn by Vottero et al. and Maghzal et al. that reduction by cyb_5 is a characteristic of all enzymes in the IDO family.

Acknowledgments This work was supported by the Australian Research Council, the National Health and Medical Research Council and the German Research Council (SFB 535, TP A12 to KB). Boniface Mailu is a scholar of the German Academic Exchange Service which is gratefully acknowledged. RS was supported by a NHMRC Senior Principal Research Fellowship, a University of Sydney Professorial Fellowship, and the University of Sydney Medical Foundation. We thank Joanne Jamie and Robert Willows of Macquarie University for use of the MUCAB CD spectrometer.

References

Austin CJD, Mizdrak J, Matin A, Sirijovski N, Kosim-Satyaputra P, Willows RD, Roberts TH, Truscott RJW, Polekhina G, Parker MW, Jamie JF (2004) Optimised expression and purification of recombinant human indoleamine 2,3-dioxygenase. Protein Expr Purif 37:392–398. doi:10.1016/j.pep.2004.06.025

Austin CJ, Astelbauer F, Kosim-Satyaputra P, Ball HJ, Willows RD, Jamie JF, Hunt NH (2009) Mouse and human indoleamine 2,3-dioxygenase display some distinct biochemical and structural properties. Amino Acids 36:99–106. doi:10.1007/s00726-008-0037-6

Ball HJ, Sanchez-Perez A, Weiser S, Austin CJD, Astelbauer F, Miu J, McQuillan JA, Stocker R, Jermiin LS, Hunt NH (2007) Characterization of an indoleamine 2,3-dioxygenase-like protein found in humans and mice. Gene 396:203–213

Ball HJ, Yuasa HJ, Austin CJ, Weiser S, Hunt NH (2009) Indoleamine 2,3-dioxygenase-2; a new enzyme in the

kynurenine pathway. Int J Biochem Cell Biol. doi:10.1016/j.biocel.2008.01.005
Beadle GW, Mitchell HK, Nyc JF (1947) Kynurenine as an intermediate in the formation of nicotinic acid from tryptophane by neurospora. Proc Natl Acad Sci USA 33:155–158. doi:10.1073/pnas.33.6.155
Calalb MB, Polte TR, Hanks SK (1995) Tyrosine phosphorylation of focal adhesion kinase at sites in the catalytic domain regulates kinase activity: a role for Src family kinases. Mol Cell Biol 15:954–963
Chen R, Li L, Weng Z (2003) ZDOCK: an initial-stage protein-docking algorithm. Proteins 52:80–87
Comeau SR, Gatchell DW, Vajda S, Camacho CJ (2004) ClusPro: a fully automated algorithm for protein-protein docking. Nucleic Acids Res 32:W96–W99
Danesch U, Hashimoto S, Renkawitz R, Schutz G (1983) Transcriptional regulation of the tryptophan oxygenase gene in rat liver by glucocorticoids. J Biol Chem 258:4750–4753
Danesch U, Gloss B, Schmid W, Schutz G, Schule R, Renkawitz R (1987) Glucocorticoid induction of the rat tryptophan oxygenase gene is mediated by two widely separated glucocorticoid-responsive elements. EMBO J 6:625–630
Delcarte J, Fauconnier M, Jacques P, Matsui K, Thonart P, Marlier M (2003) Optimisation of expression and immobilized metal ion affinity chromatographic purification of recombinant (His)6-tagged cytochrome P450 hydroperoxide lyase in *Escherichia coli*. J Chromatogr B Anal Technol Biomed Life Sci 786:229–236. doi:10.1016/S1570-0232(02)00815-2
Fallarino I, Grohmann U, Vacca C, Bianchi R, Orabona C, Spreca A, Fioretti MC, Puccetti P (2002) T cell apoptosis by tryptophan catabolism. Cell Death Differ 9:1069–1077. doi:10.1038/sj.cdd.4401073
Feis A, Marzocchi MP, Paoli M, Smulevich G (1994) Spin state and axial ligand bonding in the hydroxide complexes of metmyoglobin, methemoglobin, and horseradish peroxidase at room and low temperatures. Biochemistry 33:4577–4583. doi:10.1021/bi00181a019
Frey AB, Monu N (2008) Signaling defects in anti-tumor T cells. Immunol Rev 222:192–205. doi:10.1111/j.1600-065X.2008.00606.x
Haber R, Bessette D, Hulihangiblin B, Durcan MJ, Goldman D (1993) Identification of tryptophan 2,3-dioxygenase RNA in rodent brain. J Neurochem 60:1159–1162. doi:10.1111/j.1471-4159.1993.tb03269.x
Hansen AM, Driussi C, Turner V, Takikawa O, Hunt NH (2000) Tissue distribution of indoleamine 2,3-dioxygenase in normal and malaria-infected tissue. Redox Rep 5:112–115. doi:10.1179/135100000101535384
Hansen AM, Ball HJ, Mitchell AJ, Miu J, Takikawa O, Hunt NH (2004) Increased expression of indoleamine 2,3-dioxygenase in murine malaria infection is predominantly localised to the vascular endothelium. Int J Parasitol 34:1309–1319. doi:10.1016/j.ijpara.2004.07.008
Harrison RG, Weiner JS (1949) Vascular patterns of the mammalian testis and their functional significance. J Exp Biol 26:304–316
Heyes MP, Morrison PF (1997) Quantification of local de novo synthesis versus blood contributions to quinolinic acid concentrations in brain and systemic tissues. J Neurochem 68:280–288. doi:10.1046/j.1471-4159.1997.68010280.x
Heyes MP, Brew BJ, Saito K, Quearry BJ, Price RW, Lee K, Bhalla RB, Der M, Markey SP (1992a) Interrelationships between quinolinic acid, neuroactive kynurenines, neopterin and beta-2-microglobulin in cerebrospinal-fluid and serum of HIV-1-infected patients. J Neuroimmunol 40:71–80. doi:10.1016/0165-5728(92)90214-6
Heyes MP, Saito K, Crowley JS, Davis LE, Demitrack MA, Der M, Dilling LA, Elia J, Kruesi MJP, Lackner A, Larsen SA, Lee K, Leonard HL, Markey SP, Martin A, Milstein S, Mouradian MM, Pranzatelli MR, Quearry BJ, Salazar A, Smith M, Strauss SE, Sunderland T, Swedo SW, Tourtellotte WW (1992b) Quinolinic acid and kynurenine pathway metabolism in inflammatory and noninflammatory neurological disease. Brain 115:1249–1273
Honig A, Rieger L, Kapp M, Sutterlin M, Dietl J, Kammerer U (2004) Indoleamine 2,3-dioxygenase (IDO) expression in invasive extravillous trophoblast supports role of the enzyme for materno-fetal tolerance. J Reprod Immunol 61:79–86. doi:10.1016/j.jri.2003.11.002
Hou DY, Muller AJ, Sharma MD, DuHadaway J, Banerjee T, Johnson M, Mellor AL, Prendergasts GC, Munn DH (2007) Inhibition of indoleamine 2,3-dioxygenase in dendritic cells by stereoisomers of 1-methyl-tryptophan correlates with antitumor responses. Cancer Res 67:792–801. doi:10.1158/0008-5472.CAN-06-2925
Hunt NH, Golenser J, Chan-Ling T, Parekh S, Rae C, Potter S, Medana IM, Miu J, Ball HJ (2006) Immunopathogenesis of cerebral malaria. Int J Parasitol 36:569–582. doi:10.1016/j.ijpara.2006.02.016
Kehoe JW, Bertozzi CR (2000) Tyrosine sulfation: a modulator of extracellular protein–protein interactions. Chem Biol 7:57–61. doi:10.1016/S1074-5521(00)00093-4
Kim YH, Berry AH, Spencer DS, Stites WE (2001) Comparing the effect on protein stability of methionine oxidation versus mutagenesis: steps toward engineering oxidative resistance in proteins. Protein Eng 14:343–347. doi:10.1093/protein/14.5.343
Knox WE (1966) The regulation of tryptophan pyrrolase activity by tryptophan. Adv Enzyme Regul 4:287–297
Kuma F (1981) Properties of methemoglobin reductase and kinetic study of methemoglobin reduction. J Biol Chem 256:5518–5523
Kurokawa H, Lee DS, Watanabe M, Sagami I, Mikami B, Raman CS, Shimizu T (2004) A redox-controlled molecular switch revealed by the crystal structure of a bacterial heme PAS sensor. J Biol Chem 279:20186–20193. doi:10.1074/jbc.M314199200
Laemmli UK (1970) Cleavage of structural proteins during assembly of head of bacteriophage-T4. Nature 227:680–685. doi:10.1038/227680a0
Lyskov S, Gray JJ (2008) The RosettaDock server for local protein-protein docking. Nucleic Acids Res 36:W233–W238
Maghzal GJ, Thomas SR, Hunt NH, Stocker R (2008) Cytochrome b5, not superoxide anion radical, is a major reductant of indoleamine 2,3-dioxygenase in human cells. J Biol Chem 283:12014–12025. doi:10.1074/jbc.M710266200
Metz R, DuHadaway JB, Kamasani U, Laury-Kleintop L, Muller AJ, Prendergast GC (2007) Novel tryptophan catabolic enzyme IDO2 is the preferred biochemical target of the antitumor indoleamine 2,3-dioxygenase inhibitory compound D-1-methyl-tryptophan. Cancer Res 67:7082–7087. doi:10.1158/0008-5472.CAN-07-1872
Novak N (2006) Targeting dendritic cells in allergen immunotherapy. Immunol Allergy Clin N Am 26:307–319. doi:10.1016/j.iac.2006.02.010
Peitsch MC (1995) Protein modeling by e-mail (vol 13, pg 658, 1995). Biotechnology 13:723. doi:10.1038/nbt0895-723
Peterson AC, Migawa MT, Martin MM, Hamaker LK, Czerwinski KC, Zhang W, Arend RA, Fisette PL, Ozaki Y, Will JA, Brown RR, Cook JM (1994) Evaluation of functionalized tryptophan derivatives and related compounds as competitive inhibitors of indoleamine 2,3-dioxygenase. Med Chem Res 4:531–544
Pfefferkorn ER, Eckel M, Rebhun S (1986) Interferon-gamma suppresses the growth of *Toxoplasma gondii* in human fibroblasts through starvation of tryptophan. Mol Biochem Parasitol 20:215–224. doi:10.1016/0166-6851(86)90101-5

Schenkman JB, Jansson I (2003) The many roles of cytochrome b5. Pharmacol Ther 97:139–152. doi:10.1016/S0163-7258(02)00327-3

Shimizu T, Nomiyama S, Hirata F, Hayaishi O (1978) Indoleamine 2,3-dioxygenase—purification and some properties. J Biol Chem 253:4700–4706

Silbernagl S (1988) The renal handling of amino acids and oligopeptides. Physiol Rev 68:911–1007

Sono M (1989) The roles of superoxide anion and methylene-blue in the reductive activation of indoleamine 2,3-dioxygenase by ascorbic-acid or by xanthine oxidase-hypoxanthine. J Biol Chem 264:1616–1622

Southan MD, Truscott RJW, Jamie JF, Pelosi L, Walker MJ, Maeda H, Iwamoto Y, Tone S (1996) Structural requirements of the competitive binding site of recombinant human indoleamine 2,3-dioxygenase. Med Chem Res 6:343–352

Stone TW, Mackay GM, Forrest CM, Clark CJ, Darlington LG (2003) Tryptophan metabolites and brain disorders. Clin Chem Lab Med 41:852–859. doi:10.1515/CCLM.2003.129

Sugimoto H, Oda S, Otsuki T, Hino T, Yoshida T, Shiro Y (2006) Crystal structure of human indoleamine 2,3-dioxygenase: catalytic mechanism of O-2 incorporation by a heme-containing dioxygenase. Proc Natl Acad Sci USA 103:2611–2616. doi:10.1073/pnas.0508996103

Suzuki T, Kawamichi H, Imai K (1998) A myoglobin evolved from indoleamine 2,3-dioxygenase, a tryptophan-degrading enzyme. Comp Biochem Physiol B Biochem Mol Biol 121:117–128. doi:10.1016/S0305-0491(98)10086-X

Suzuki S, Tone S, Takikawa O, Kubo T, Kohno I, Minatogawa Y (2001) Expression of indoleamine 2,3-dioxygenase and tryptophan 2,3-dioxygenase in early concepti. Biochem J 355:425–429. doi:10.1042/0264-6021:3550425

Takikawa O, Kuroiwa T, Yamazaki F, Kido R (1988) Mechanism of interferon-gamma action—characterization of indoleamine 2,3-dioxygenase in cultured human-cells induced by interferon-gamma and evaluation of the enzyme-mediated tryptophan degradation in its anticellular activity. J Biol Chem 263:2041–2048

Tankiewicz A, Pawlak D, Topczewska-Bruns J, Buczko W (2003) Kidney and liver kynurenine pathway enzymes in chronic renal failure. Adv Exp Med Biol 527:409–414

Terentis AC, Thomas SR, Takikawa O, Littlejohn TK, Truscott RJW, Armstrong RS, Yeh SR, Stocker R (2002) The heme environment of recombinant human indoleamine 2,3-dioxygenase—structural properties and substrate-ligand interactions. J Biol Chem 277:15788–15794. doi:10.1074/jbc.M200457200

Thomas SR, Stocker R (1999) Redox reactions related to indoleamine 2,3-dioxygenase and tryptophan metabolism along the kynurenine pathway. Redox Rep 4:199–220. doi:10.1179/135100099101534927

Thomas SR, Terentis AC, Cai H, Takikawa O, Levina A, Lay PA, Freewan M, Stocker R (2007) Post-translational regulation of human indoleamine 2,3-dioxygenase activity by nitric oxide. J Biol Chem 282:23778–23787. doi:10.1074/jbc.M700669200

Unneberg P, Merelo JJ, Chacon P, Moran F (2001) SOMCD: method for evaluating protein secondary structure from UV circular dichroism spectra. Proteins Struct Funct Genet 42:460–470. doi:10.1002/1097-0134(20010301)42:4<460:AID-PROT50>3.0.CO;2-U

van Gunsteren WF, Billeter SR, Eising A, Hünenberger PH, Krüger P, Mark AE, Scott WRP, Tironi IG (1996) Biomolecular simulations: the GROMOS96 manual and user guide. VdF Hochschulverlag ETHZ, Zürich

Vottero E, Mitchell DA, Page MJ, MacGillivray RTA, Sadowski IJ, Roberge M, Mauk AG (2006) Cytochrome b5 is a major reductant in vivo of human indoleamine 2,3-dioxygenase expressed in yeast. Febs Lett 580:2265–2268. doi:10.1016/j.febslet.2006.03.034

Williams CA, Harry RA, McLeod JD (2007) Apoptotic cells induce dendritic cell-mediated suppression via interferon-gamma-induced IDO. Immunology. doi:10.1111/j.1365-2567.2007.02743.x

World Health Organization (1999) WHO laboratory manual for the examination of human semen and sperm-cervical mucus interaction, 4th edn. Published on behalf of the World Health Organization by Cambridge University Press, Cambridge, UK, 128 p

Yuasa HJ, Takubo M, Takahashi A, Hasegawa T, Noma H, Suzuki T (2007) Evolution of vertebrate indoleamine 2,3-dioxygenases. J Mol Evol 65:705–714. doi:10.1007/s00239-007-9049-1